Preventing Salt Formation in Zero-Gap CO$_2$ Electrolyzers by Quantifying Cation Accumulation

Biemolt, Jasper; Singh, Jai; Prats Vergel, Gerard; Pelzer, Henri M.; Burdyny, Thomas

Important note
To cite this publication, please use the final published version (if applicable).
Please check the document version above.

LETTER

Preventing Salt Formation in Zero-Gap CO_2 Electrolyzers by Quantifying Cation Accumulation

Jasper Biemolt, Jai Singh, Gerard Prats Vergel, Henri M. Pelzer, and Thomas Burdyny*

Read Online

ACCESS | Metrics & More | Article Recommendations | SI Supporting Information

ABSTRACT: The electrochemical CO_2 reduction reaction (CO_2RR) in a membrane electrode assembly (MEA) efficiently turns CO_2 into a feedstock. However, unfavorable steady-state concentrations of ions in the cathode compartment result in salt formation if unaddressed, which restricts the access of CO_2 and causes cell failure. Here, we systematically show the relationship between salt accumulation and four system parameters including cation species, anolyte concentration, membrane thickness, and operating temperature. To compare each metric, we quantified the cation accumulation rate at predefined operating times. Notably, we show that operating at temperatures above 50 °C with properly humidified CO_2 stream fully avoids salt formation. We further show that combining separate operating conditions is also highly effective, showing operation for >144 h with no measurable salt deposition at 200 mA/cm². Collectively, our work systematically demonstrates that salt formation is a prevalent yet surmountable CO_2RR challenge that can be overcome by elevated cell temperatures or switching to more soluble alkali cations.

Zero-gap CO_2 electrolyzer

Tapping into carbon dioxide (CO_2) as an industrial feedstock for carbon-based compounds is a necessary but substantial challenge for a circular economy.[1,2] Due to CO_2's inherent stability, the initial conversion step is particularly energy demanding. The electrochemical CO_2 reduction reaction (CO_2RR) is one means of utilizing electrical energy to break apart CO_2.[3−5] Efficient and relevant CO_2RR rates are reached through zero-gap membrane electrode assemblies (MEA).[6,7] Here, the poor aqueous solubility of CO_2 is overcome through a gas−liquid interface near the catalyst layer, with the short diffusion pathways of CO_2 maintained by gas diffusion electrodes (GDE).[8,9] In these reactor configurations, near-unity selectivity toward CO_2RR can be achieved near ampere-level current densities with modest energy efficiencies.[10−13]

Under such conditions, however, CO_2 can also react with alkaline CO_2RR byproducts (OH^- in eq 1) to create a local alkaline environment favorable for the formation of (bi)-carbonate salts (eq 2).[14−16] Salt formation occurs when the carbonate produced at the cathode sufficiently accumulates, and pairs with cations migrating across the anion exchange membrane (AEM), exceeding the solubility limit.[17,18] Ideally, all anions formed at the cathode would migrate across the AEM without accumulating, while cations would be rejected by

the AEM's fixed charges. Yet, cations do migrate over the AEM and the resulting salt formation blocks CO_2 flow to the catalyst, resulting in decreased Faradaic efficiencies, and can further build up pressure in the gas channel.[17,19] Such salt-related failure of the CO_2RR systems is untenable for industrial operation.

$$CO_2 + H_2O + 2e^- \rightarrow CO + 2OH^- \tag{1}$$

$$CO_2 + 2OH^- + 2K^+ \rightarrow K_2CO_3 + H_2O \tag{2}$$
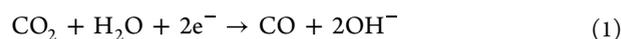
Cation and (bi)carbonate concentration management at the cathode is thus crucial in preventing salt formation, as at the most standard MEA operation conditions (>200 mA cm⁻²), salt related time-of-failure is a few hours. Several delaying approaches have been proposed, as we describe in our recent perspective on this subject,[17] translating into four key operational parameters for salt prevention: cation species,[20]
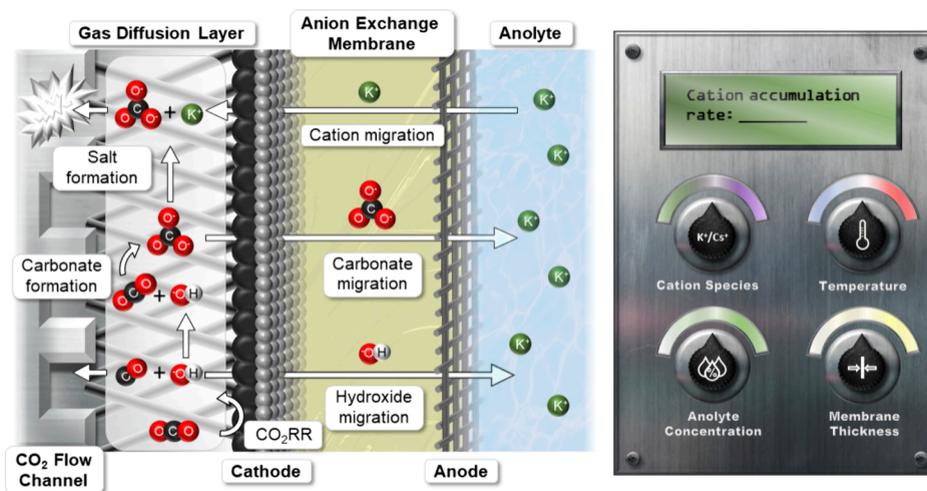
Figure 1. The electrochemical and chemical reaction pathway leading to salt formation in the cathode of a CO_2 electrolyzer (left). A representation of the strongest control knobs to mitigate salt formation by enabling improved ionic transport (right).

anolyte concentration,[21] temperature,[22] and membrane transport properties (Figure 1).[23] These operational conditions positively impact ion accumulation and transport phenomena, which are described through electroneutrality and the Nernst−Planck equation:

$$J_i(x, t) = -D_i \frac{\partial C_i(x, t)}{\partial x} + \frac{-D_i z_i F}{RT} C_i(x, t) \frac{\partial \varphi(x, t)}{\partial x} + C_i v(x, t) \qquad (3)$$

flux = diffusion + migration + advection

where J_i is the flux of ions, D_i is the ion's diffusivity constant, C_i is the ionic concentration, z_i is the ion's electronic charge, F is Faraday's constant, R is the ideal gas constant, T is the temperature, ϕ is the electric potential, and v is the fluid velocity. In a zero-gap MEA cell, the advection component is negligible. Thus, ion transport is heavily determined by the cell's potential gradient (migration), the anode-to-cathode concentration gradient (diffusion), and the Donnan exclusion factor of the AEM (membrane transport properties).[24,25] Separate from transport phenomena, the solubility product is further influenced by temperature and cation species.[26]

A few rigorous studies have tried to provide quantitative salt-related cell failure comparisons in MEA systems. For example, Cofell et al. determined the location and degree of salt precipitation for different anolytes, including different alkali cations, hydroxides, and (bi)carbonates, through post-mortem scanning electron microscopy of the GDE.[16] Similarly, Garg et al. further analyzed the entire GDE with operando wide-angle X-ray scattering at different anolyte concentrations and alkali cation species.[20] The highlighted precipitation locations at the different operational conditions agreed well with the work of Disch et al.[27] Kong et al. also elucidated the salt precipitation location in the GDE using energy-dispersive X-ray mapping yet combined it with inductively coupled plasma mass spectrometry to determine the salt accumulation.[28] Importantly, most studies compared different time-to-failures for mostly one or two operational parameters, where the analysis of salt precipitation was qualitative. To accurately determine the effectiveness of a variety of operational conditions (e.g., cation concentration/species, temperature, etc.) in salt formation, a quantitative measure of salt formation is required.[29] Preferably,

this methodology can track ion buildup on short time scales and yield an indication of the potential of the cell to suffer from salt-related cell failure. Only then can we come to a combined approach which fully overcomes salt precipitation as a challenge plaguing CO_2 electrolysis at various current densities.

Here, we quantified cation accumulation rates at the cathode of a zero-gap CO_2 electrolyzer over a broad parameter space consisting of anolyte concentration, cation species, membrane transport properties, and temperature. Despite the complex transport phenomena, we show how the cation accumulation varies with each of the parameters, offering a predictive value for the potential of the cell to suffer from salt-related cell failure, through only a simple 2-h experiment. Simultaneously, we identify the conditions that are most likely to mitigate salt formation in CO_2 electrolyzers entirely. For example, raising the cell temperature has the greatest effect, reducing cation accumulation rates by 50-fold (from 3.6 to 0.08 μmol K^+ min^{-1} cm^{-2}), while fully avoiding salt formation over the examined time period. Last, we show that combining two or more salt mitigation strategies together (e.g., cesium-based anolyte + thinnest membrane) provides a substantially reduced cation accumulation rate (from 0.12 to 0.032 μmol Cs^+ min^{-1} cm^{-2}) and thus lowered the potential for the cell to suffer salt-related cell failure. We show a complete avoidance of salt formation over 144 h at a current density of 200 mA cm^{-2}, while maintaining a high anolyte concentration.

A challenge to overcoming salt formation is first through its quantification. There are several options to quantify salt related time-to-failure besides the earlier mentioned post-mortem scanning electron microscopy and operando wide-angle X-ray scattering, each with their own merits. Monitoring electrode potential, Faradaic efficiency (FE), gas flows, and pressures can all identify cycles of salt formation and flow channel blockage, for example (Figure S1). These means are qualitative and indirect regarding the actual salt formation itself, however, and do not yield a quantitative measure of the salt accumulation. For example, changes to FE or pressures may only occur after substantial salt precipitation throughout the flow channel, yet the same changes will occur through a small amount of salt blockages at the inlet of the reactor. Thus, correlating trends in failure time with varied parameters using only qualitative salt
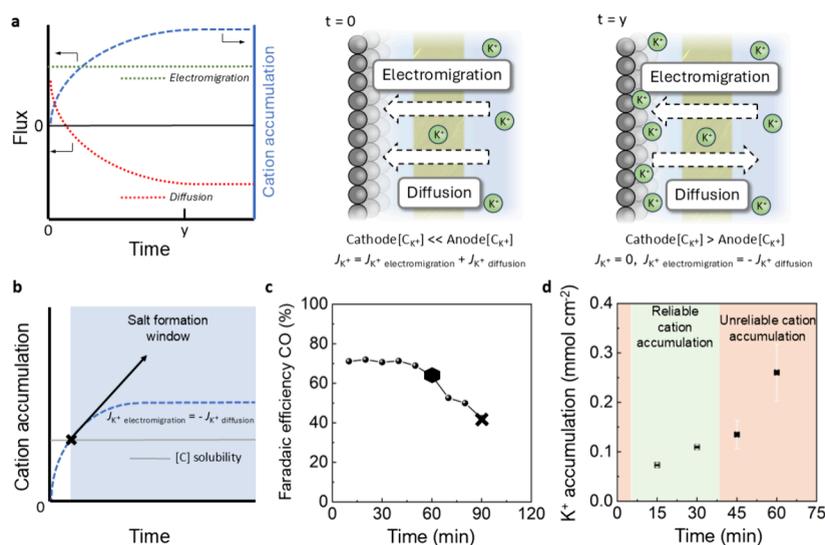
Figure 2. (a) A sketch of the diffusion and migration fluxes, and the total cation accumulation over time, with representations of the environments and flux contributions at different times. (b) The deviation of the cation accumulation (solid black arrow, representing the continuous accumulation of cations) from the theoretic accumulation line (dashed blue line), based on a solubility limit; (c) the cell lifetime depicted by the Faradaic efficiency toward CO for a cell operated with 0.5 M KHCO$_3$ (where the ✕ marks the failure moment at which the flow rate was obstructed by salt formation, while a ⬢ mark indicates a salt-related flooding phenomenon); and (d) the potassium cation concentration from the flushed cathode channels over the course of multiple experiments, average over two experiments with the error bar (gray) representing the standard.

indicators is then challenging due to large statistical variation in salt formation location and the criticalness of the location to cell operation. Additionally, these qualitative salt formation measurements through traditional means may require operating for 50−100 h. Systematically evaluating a large parameter space with such long experiments combined with variability is then experimentally onerous. Thus, a better approach is needed.

As an alternative approach to quantifying salt formation, we instead focus on the direct measurement of the cation accumulation rate in the cathode compartment. In theory, the cationic accumulation over time follows a logarithmic curve, sketched in Figure 2a, that plateaus at a concentration level at which the electromigration and diffusion terms become equal (equalization concentration). While in a zero-gap configuration the initial cationic concentration at the cathode is zero, the rapid concentration increase at the cathode induces a cation back-diffusion over the membrane. Salt formation thus occurs when the equalization concentration is above the solubility product (Figure 2b), where the rate of salt formation is constant (any additional flux goes out of the cathode−membrane interface as salt without altering steady state). In this regard, our studied operational parameters (e.g., anolyte concentration, cation species, membrane transport properties, and temperature) either increase the solubility limit or alter the equalization concentration (by affecting electromigration and/or back-diffusion). The closer the solubility limit and equalization concentration are to each other, the less likely salt-related cell failure occurs and consequently translates to a lower cathode cation buildup. We can thus use the cation accumulation rate to compare the effectiveness of the operational parameters on reducing the potential to suffer from salt-related cell failure.

We can measure the cation accumulation by flushing a fixed aqueous volume through the cathode compartment (including the cathode and cathode flow channels) and determine the

buildup of cations by ion chromatography. This method is similar to the method of Kong et al., who used soaking the GDE in a fixed aqueous volume combined with inductively coupled plasma mass spectrometry to determine the salt accumulation.[28] Assuming electroneutrality, the cation buildup is correlated with the accumulation of (bi)carbonate species. Yet, we do not want to assume that the salt accumulation determination will be reliable within the entire cell operation window. As such, we measured cation accumulation at different 15 min intervals (through separate experiments) for an experiment that we know exhibits salt-related flooding after ∼60 min and catastrophic failure after 90 min (Figure 2c). As shown in Figure 2d, the cation accumulation has a significantly low error margin at 15 and 30 min, where we assume a reproducible quasi-steady state in ionic transport. Yet, the cation accumulation becomes unreliable between 45 and 60 min, coinciding with the first performance-based signs of salt formation in Figure 2c, as the formed salt alters the GDE flooding state, main charge carrier, and the local electrode environment (breaking the established quasi-steady between diffusion and electromigration). Our quantification of the cation accumulation rate should thus be performed before extreme salt formation occurs (before full cell failure).

Our established protocol is thus usable within the initial period of an experiment, where the cation accumulation rate correlates to the potential of the cell to suffer from salt related-cell failure in the long term. When possible, the cation accumulation rates are measured within the first 2 h of an experiment to yield a better comparability. An important caveat about the cation accumulation methodology, however, is that rinsing of the gas channel may not dissolve all salts or ionic species present within the gas-diffusion layer (due to the hydrophobic nature of the macro- and microporous layers). The method is then biased toward salt deposition in the gas channel. Previous work has shown though that salt formation begins at the catalyst layer and moves gradually into the micro-
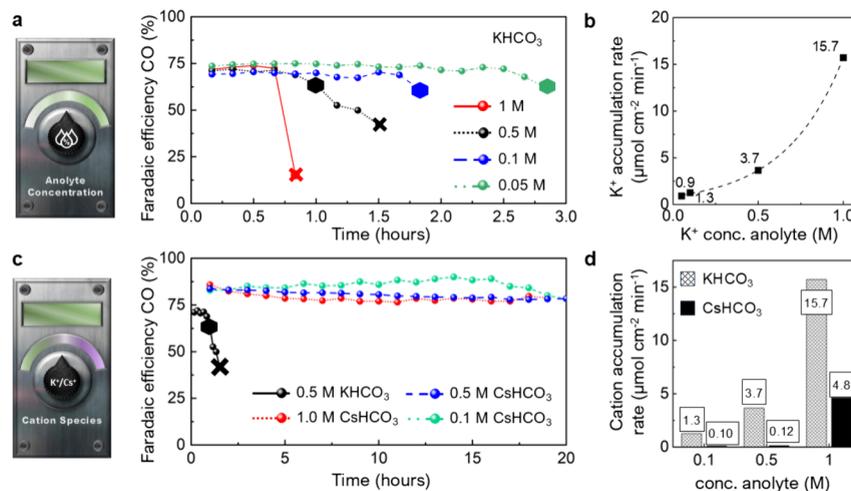
Figure 3. (a) The cell lifetime and (b) cation accumulation at different anolyte concentrations and (c) lifetime of cells operated with cesium and potassium bicarbonate anolytes and (d) cation accumulation rates of cesium and potassium bicarbonate anolytes with different concentrations. See Tables S1 and S3 for the cell and cation accumulation conditions. The ✕ marks the failure moment at which the flow rate was obstructed by salt formation, while a ⬡ mark indicates a salt-related flooding phenomenon.

and macroporous layers due to flooding and diffusion effects.[16,30] Thus, cation accumulation measurements taken in the first couple of hours for very low accumulation rates are likely less accurate than scenarios that see salt formation earlier.

We then charted the cation accumulation rates at different operational conditions (anolyte concentration, cation species, membrane thickness, and temperature) using our developed methodology, primarily focusing on determining the separate and combined sensitivity of salt formation for each parameter. All cell conditions and components are kept the same except for the parameter under investigation (see Supporting Information, Table S1). The baseline parameters then consist of a 0.5 M $KHCO_3$ anolyte, a 50-μm-thick Sustainion membrane, ambient operating temperature, and a current density of 200 mA cm^{-2}. As a benchmark for our cation accumulation measurements, separate experiments were performed until salt-related cell failure (e.g., blockage of GDE gas channels and/or sudden >10% drop in CO Faradaic efficiency), so we can correlate at which cation accumulation rate no salt-related cell failure occurs. We want to emphasize that completely predicting time-until-failure is not possible through the cation accumulation rate, as salt-related cell failure is variable. Cation accumulation rates do predict the vulnerability of cells to have salt-related cell failure and are indicative of the operational time.

As cations come from the anolyte, altering the anolyte concentration is one of the easiest ways to decrease cation accumulation,[20] as the diffusion flux (eq 3) is reduced by the higher concentration gradients between the cathode and anode (mind again that the cathode cation concentration during the experiment is close to the solubility limit). As shown in Figure 3a, a nonlinear relationship between cation concentration and failure time is observed when varying anolyte concentrations (0.05, 0.1, 0.5, and 1 M $KHCO_3$). A separate set of experiments measured the cation accumulation on shorter time scales (see Table S3). The cation accumulation in Figure 3b confirms the nonlinear behavior, but the nonlinearity is not easily explained through eq 3. The exact modeling of this nonlinear behavior is outside of the scope of this work. However, Petrov et al. showed a logarithmic dependence of the

permselectivity on the concentration gradient for Sustainion,[31] resulting in a decreased cation migration at lower concentrations. This combined with the higher diffusion rate when lowering the concentration would follow an exponential line.

From Figure 3a and b, a direct comparison between cell lifetimes and cation accumulation rates is not possible as the exact failure mechanism is not the same for each cell. At high anolyte concentrations (1 M $KHCO_3$, Figure S2a), complete CO_2 blockage accounts for cell failure. At 0.5 M $KHCO_3$ (Figure S2b), a salt-related flooding mechanism occurs just prior to a critical blockage of the flow channels. Low anolyte concentrations (0.1 and 0.05 M $KHCO_3$, Figure S2c and d) suffer mainly from salt-related cell flooding. This oscillatory response is related to salt formation yet sets in before salt reaches the cathode flow channel and blocks the system.[19] Cell failure thus does not always follow a fixed amount of cation accumulation, making an exact estimation of the operational time using cation accumulation impossible. Still, the comparison between Figure 3a and b indicates that cation accumulation rates of ~1 μmol cm^{-2} min^{-1} are substantial enough to result in a degree of salt-related failure. As the exponential trend converges to a value of 0.8 μmol cm^{-2} min^{-1}, we can conclude that lowering the anolyte concentration alone will still cause salt-related cell failure. Furthermore, lowering the anolyte concentration leads to an increased cell potential (3.6 V at 1.0 M $KHCO_3$ to 3.9 V at 0.05 M $KHCO_3$, Table S2), lowering the energy efficiency of the system. These two reasons (convergence to a value still capable of causing salt-related cell failure and the increased cell voltage) make lowering the anolyte concentration alone an unviable salt mitigation strategy for potassium-based MEA CO_2 electrolyzers.

The next parameter examined is switching the cation species from K^+ to Cs^+. Often, the increased solubility for Cs-based bicarbonates (10.78 M) versus potassium (3.62 M) is used to explain their better performance.[26] Yet, the carbonate salts share the same solubility of ~8.0 M, yielding a possible negligible effect for cesium. Still, $CsHCO_3$ as an anolyte provides an additional advantage of better CO_2RR selectivity.[32,33] Sodium and lithium are omitted here, as both will show inferior solubility and CO_2RR selectivity. The time-to-
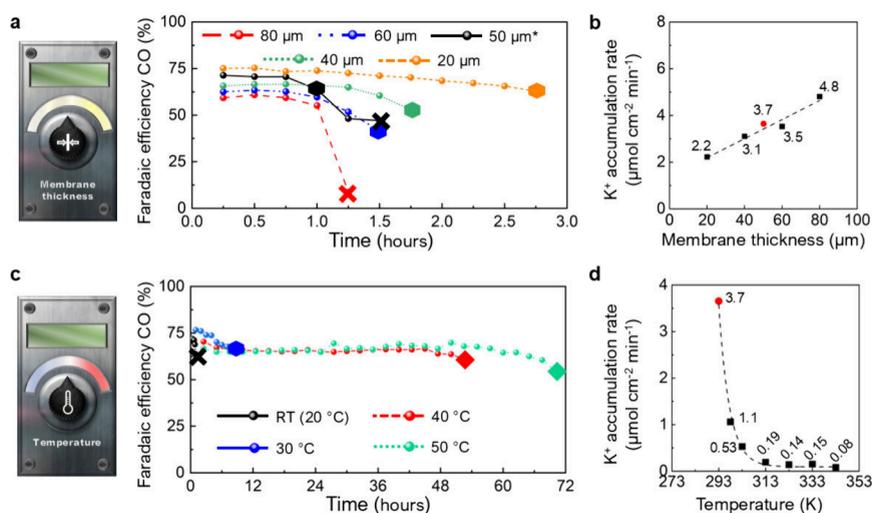
Figure 4. (a) The cell lifetime (* representing the Sustainion cell) and (b) the cation accumulation rates for different Piperion (■) and Sustainion (●) membrane thicknesses and (c) the cell lifetime at room temperature (RT) and 40 °C and (d) the cation accumulation rates at different cell temperatures (with ● representing the cell operated outside the oven). RT assumed at 20 °C. See Table S1 and S3 for the cell and cation accumulation conditions. The × marks the failure moment at which the flow rate was obstructed by salt formation, while a ⬣ mark indicates a salt-related flooding phenomenon and ◆ indicates pure flooding.

failure experiment in Figure 3c indicates, at minimum, a 20-fold extension of the cell lifetime (to 20 h), when switching from 0.5 M KHCO₃ to 1.0 M CsHCO₃, with no observable cell failure within this time frame (Figure S3). Furthermore, when the cell is opened, no salt crystals are observed at the back of the GDE or the flow channels, while a significant volume of water was collected in the liquid trap. Similar results were observed when decreasing the CsHCO₃ concentration. Interestingly, the cation accumulation rate for the 1.0 M CsHCO₃ cell exceeds the 3.7 μmol cm^{-2} min^{-1} of 0.5 M potassium, with a value of 4.6 μmol cm^{-2} min^{-1} (Figure 3d). While we cannot fully elucidate why cesium cells do not suffer from salt-related cell failure under our conditions, as this lays outside the scope of this work, the observed liquid in the liquid trap points to accumulated cesium leaving the cell in a dissolved state. The cation accumulation rate as a function of anolyte concentration follows a trend similar to that of the potassium-based cells, with lower concentrations significantly lowering the cation accumulation rates. It is noteworthy that these results are not explainable through the differences in solubility of potassium and cesium salts considering the salt failure of the 0.1 M KHCO₃ cell but no failure for the 1 M CsHCO₃ cell. Overall, using cesium comes with a slightly lowered cell voltage of 3.5 V, higher Faradaic efficiency to CO, and thus significantly enhanced energy efficiency.

The least studied cell component in relation to salt-related cell failure is the anion exchange membrane (AEM) and, in particular, the AEM thickness. Both the diffusion and electromigration terms in eq 3 depend on the distance (Δx), with this distance being governed by the membrane thickness. We used the Piperion membrane family with different commercially available thicknesses, in addition to a standard Sustainion case. We observe an increased lifetime for decreasing membrane thicknesses (Figure 4a). Additionally, Figure S4a−d show an accompanying trend of an increased CO and diminished formate Faradaic efficiency (the missing Faradaic efficiency fraction in silver-based CO₂RR is often attributed to formate). The altered Faradaic efficiencies underline a distinct variation of the local electrode environ-

ment based on the membrane thickness, agreeing with both the theoretic study by McCallum et al. and practical study by Reyes et al.[34,35] However, an in-depth explanation is beyond the scope of this paper.

The cation accumulation rate increases linearly with the membrane thicknesses (Figure 4b). Interestingly, the cation accumulation rate for Sustainion (50 μm) fits within the Piperion data remarkably well, countering our initial hypothesis of Piperion outperforming Sustainion based on its higher permselectivity.[36] Simultaneously, our data indicate no connection to a possible lower permselectivity for thinner membranes, agreeing with the distinct threshold observed by Zhang et al.[37] Our data reveal that the linear relationship between distance and (back-)diffusion in eq 3 dominates, supported by the potential gradient not being affected by the membrane thickness (see Supporting Information for explanation). We do note that in the time-until-failure experiment, Sustainion does not exactly fit the apparent trend. Here, we argue that the difference in membrane water-uptake plays a key role during the salt-related flooding phenomena. The results also highlight that, while a thinner membrane helps in lowering the cation accumulation rate, by itself, it would require extremely thin membranes to effectively reduce cation accumulation to manageable levels. Yet, thinner membranes do enhance the CO Faradaic efficiency and lower the cell potential (Table S2), with these two effects combined enhancing the energy efficiency of the cell.

Last, the cell temperature plays a complex role in cation accumulation and associated salt-related cell failure. Going from room temperature to 30 °C, we see an increased cell lifetime (Figure 4c) where the failure now occurs through salt-related flooding indicated by the observed oscillations (Figure S6a). Further increasing the temperature to 40 °C shows a ∼50-fold prolonged lifetime. At the end of the test, small salt deposits were observed at the CO₂ gas inlet, indicating the difficulty with CO₂ gas humidification at high temperatures. Yet, no oscillation in the CO FE is observed (Figure S6b) and now a nonsalt-related flooding is the failure mechanism. This trend is extended at 50 °C, only showing a limited increase in
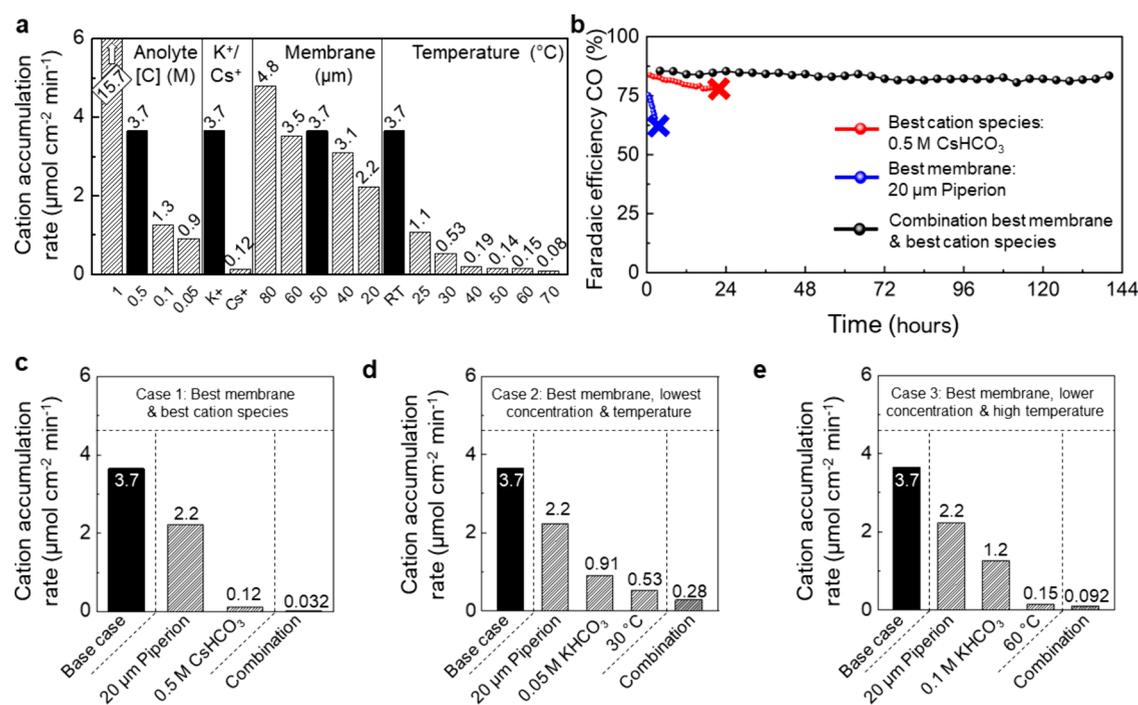
Figure 5. (a) A summary of the cation accumulation rates at our studied operation conditions. The case 1 (b) cell lifetime and (c) cation accumulation rates for a combination of 20 μm Piperion membrane and 0.5 M CsHCO$_3$ anolyte. The cation accumulation rate for (d) case 2, comprising a 20 μm Piperion membrane, 0.05 M KHCO$_3$ anolyte, and 30 °C cell temperature, and (e) case 3, comprising a 20 μm Piperion membrane, 0.1 M KHCO$_3$ anolyte, and 60 °C cell temperature. See Tables S1 and S3 for the cell and cation accumulation conditions. The $\times$ marks the failure moment at which the flow rate was obstructed by salt formation.

cell lifetime compared to the 40 °C cell, with neither observable salt in the flow channel nor oscillations in the cell performance (Figure S6c). Accordingly, the plateau in the cation accumulation rates (Figure 4d) indicates a tremendous drop in the accumulation rate already above 30 °C. As we see flooding as the main failure mode above 50 °C, we did not perform long-term experiments at higher temperatures, and the cation accumulation rates suggest the approach of a plateau in cation accumulation at 0.08 μmol cm^{-2} min^{-1}, thus diminishing the effects. Still, as salt is not observed at these high temperatures, we can speculate from Figure 4c and d, that cation accumulation at 0.08 μmol K$^+$ cm^{-2} min^{-1} is likely to mitigate salt formation.

The effect of the temperature on the cation flux is multifold. For one, the electromigration is inversely proportional to the temperature ($1/T$), further reduced by an increased membrane conductivity at higher temperatures (Table S3). While the diffusivity (D) is also temperature-dependent, it would impact both electromigration and diffusion equally for the same ionic species. The cation back-diffusion will be enhanced by the increased (bi)carbonate solubilities at elevated temperatures.[38] Additionally, the higher water load of the CO$_2$ gas stream at elevated temperatures may lead to periodic dissolution of small salt deposits, flushing the cathode compartment. Despite the complex effects on the flux, Figure 4d suggests that the greatest individual parameter for mitigating salt formation is elevated cell temperatures. Regarding other cell performance metrics, temperature is the only factor with both a positive and negative effect on overall cell performance. As the cell temperature is increased, the cell potential (Table S2) decreases, yet, above 30 °C we see a diminished Faradaic efficiency toward CO (Figures 4c and S6a−c).

As shown in Figures 2−4, only elevated temperatures and going towards cesium-based anolytes were able to significantly mitigate salt-related failure at 200 mA cm^{-2}. Furthermore, comparing all cation accumulation rates against each other in Figure 5a indicates that cation species and temperature are the most sensitive parameters, with the common denominator being enhanced solubility. We then aimed to combine effects of the separate parameters, as we anticipate cumulative effects for combinations based on the idea that transport phenomena and steady-state local ion concentrations drive salt formation conditions. The three different combinations below illustrate the combinatorial benefits.

In case 1, we reflect on the combinatorial benefits for cesium. While salt formation does not occur for this cation species under our conditions, cations that migrated to the cathode must still be recycled back to the anolyte reservoir in an industrial process. As such, limiting the cation accumulation is still of interest. Here, we then combined cesium (0.5 M CsHCO$_3$) with the best membrane (20 μm Piperion). As shown in Figures 5b and S7a,b, the combined parameters in case 1 achieved continuous operation for 144 h with no signs of salt-related cell failure or flooding, with the test being stopped manually. Neither anolyte replacement nor cathode gas channel flushing was required. Case 1 achieves a significant improvement compared to individual base cases with a cation accumulation rate of only 0.032 μmol cm^{-2} min^{-1} (Figure 5c). From case 1, we can again conclude that cesium-based CO$_2$ zero-gap AEM MEA electrolyzers do not require elevated temperatures to run without salt-related cell failure. As such, we also tested no other combinations using cesium, as any further improvement is not necessary.

Case 2 pairs the best membrane (20 μm Piperion), lowest anolyte concentration (0.05 M KHCO$_3$), and slightly increased

cell temperature (30 °C), aiming to answer the question of whether a potassium-based cell can operate without critical salt formation without requiring elevated temperatures. The cation accumulation rate of 0.28 μmol cm^{-2} min^{-1} (Figure 5d) reveals still a significant salt formation tendency of this cell, being larger than the elevated temperature cases. Based on the cation accumulation rates of the elevated temperature cases, a rate of 0.28 μmol cm^{-2} min^{-1} is still likely to facilitate salt-related cell failure. Additionally, operating at low anolyte concentration results in an initial oscillation in CO/H_2 Faradaic efficiencies (Figure S8a) and potentials (Figure S8b). We can thus conclude that salt mitigation is possible only at elevated temperatures for potassium-based CO_2 electrolyzers.

To see how effective combining different salt mitigation strategies are at elevated temperatures, we combined the best membrane (20 μm Piperion membrane), lower anolyte concentration (0.1 M $KHCO_3$) and high temperature (60 °C) in case 3. As we know, salt-related cell failure will likely not occur (we already did not see salt-related cell failure at 50 °C), so we focused purely on the cation accumulation rate. We could still observe a lowered cation accumulation rate compared to solely running at 60 °C (Figure 5e), however at diminishing returns (only a 39% decrease compared to the 60 °C parameter). In this sense, the optimized conditions still aid in reducing the frequency of anolyte replenishment.

In this work, we showed the effectivity of cathode cation accumulation as an indicator for salt-related cell failure, using this to determine the effect of four key operating conditions (anolyte concentration, cation species, membrane thickness, and cell temperature) on the cell lifetime of zero-gap CO_2 electrolyzers. We observed the lowest cation accumulation when increasing the overall salt solubility, either through elevated temperatures (50-fold reduction) or highly soluble alkali cations (30-fold reduction). Combining the optimized parameters reduces the cation accumulation rate further, with the rates converging to a singular value. In the end, 144 h of cell operation was demonstrated without salt formation. These results highlight that salt formation in the CO_2RR is a solvable challenge with the right operating parameters.

ASSOCIATED CONTENT

Ⓢ Supporting Information

The Supporting Information is available free of charge at https://pubs.acs.org/doi/10.1021/acsenergylett.4c03242.

> Details about the performed electrochemical and cation accumulation experiments, tabulated data about the experimental conditions examined, tabulated experimental data, and time-resolved Faradaic efficiency data supporting the main text figures (PDF)

AUTHOR INFORMATION

Corresponding Author

Thomas Burdyny − *Materials for Energy Conversion and Storage (MECS), Department of Chemical Engineering, Faculty of Applied Sciences, Delft University of Technology, Delft 2629 HZ, The Netherlands;* ⓞ orcid.org/0000-0001-8057-9558; Email: T.E.Burdyny@tudelft.nl

Authors

Jasper Biemolt − *Materials for Energy Conversion and Storage (MECS), Department of Chemical Engineering, Faculty of*

Applied Sciences, Delft University of Technology, Delft 2629 HZ, The Netherlands

Jai Singh − *Materials for Energy Conversion and Storage (MECS), Department of Chemical Engineering, Faculty of Applied Sciences, Delft University of Technology, Delft 2629 HZ, The Netherlands*

Gerard Prats Vergel − *Materials for Energy Conversion and Storage (MECS), Department of Chemical Engineering, Faculty of Applied Sciences, Delft University of Technology, Delft 2629 HZ, The Netherlands*

Henri M. Pelzer − *Materials for Energy Conversion and Storage (MECS), Department of Chemical Engineering, Faculty of Applied Sciences, Delft University of Technology, Delft 2629 HZ, The Netherlands*

Complete contact information is available at:
https://pubs.acs.org/10.1021/acsenergylett.4c03242

Notes

The authors declare no competing financial interest.

REFERENCES

(1) Theofanidis, S. A.; Antzaras, A. N.; Lemonidou, A. A. CO2 as a Building Block: From Capture to Utilization. *Curr. Opin. Chem. Eng.* **2023**, *39*, 100902.

(2) Sharifian, R.; Wagterveld, R. M.; Digdaya, I. A.; Xiang, C.; Vermaas, D. A. Electrochemical Carbon Dioxide Capture to Close the Carbon Cycle. *Energy Environ. Sci.* **2021**, *14* (2), 781−814.

(3) Jin, S.; Hao, Z.; Zhang, K.; Yan, Z.; Chen, J. Advances and Challenges for the Electrochemical Reduction of CO2 to CO: From Fundamentals to Industrialization. *Angew. Chem.* **2021**, *133* (38), 20795−20816.

(4) Costentin, C.; Robert, M.; Savéant, J.-M. Catalysis of the Electrochemical Reduction of Carbon Dioxide. *Chem. Soc. Rev.* **2013**, *42* (6), 2423−2436.

(5) Overa, S.; Ko, B. H.; Zhao, Y.; Jiao, F. Electrochemical Approaches for CO2 Conversion to Chemicals: A Journey toward Practical Applications. *Acc. Chem. Res.* **2022**, *55* (5), 638−648.

(6) Endrődi, B.; Bencsik, G.; Darvas, F.; Jones, R.; Rajeshwar, K.; Janáky, C. Continuous-Flow Electroreduction of Carbon Dioxide. *Prog. Energy Combust. Sci.* **2017**, *62*, 133−154.

(7) Zhang, Z.; Huang, X.; Chen, Z.; Zhu, J.; Endrődi, B.; Janáky, C.; Deng, D. Membrane Electrode Assembly for Electrocatalytic CO$_2$ Reduction: Principle and Application. *Angew. Chem., Int. Ed.* **2023**, *62* (28), No. e202302789.

(8) Burdyny, T.; Smith, W. A. CO2 Reduction on Gas-Diffusion Electrodes and Why Catalytic Performance Must Be Assessed at Commercially-Relevant Conditions. *Energy Environ. Sci.* **2019**, *12* (5), 1442−1453.

(9) Nguyen, T. N.; Dinh, C.-T. Gas Diffusion Electrode Design for Electrochemical Carbon Dioxide Reduction. *Chem. Soc. Rev.* **2020**, *49* (21), 7488−7504.

(10) Ma, Z.; Wang, B.; Yang, X.; Ma, C.; Wang, W.; Chen, C.; Liang, F.; Zhang, N.; Zhang, H.; Chu, Y.; Zhuang, Z.; Xu, H.; Wang, Y.; Liu, J. P-Block Aluminum Single-Atom Catalyst for Electrocatalytic CO2 Reduction with High Intrinsic Activity. *J. Am. Chem. Soc.* **2024**, *146* (42), 29140−29149.

(11) Liang, Y.; Li, F.; Miao, R. K.; Hu, S.; Ni, W.; Zhang, S.; Liu, Y.; Bai, Y.; Wan, H.; Ou, P.; Li, X.-Y.; Wang, N.; Park, S.; Li, F.; Zeng, J.; Sinton, D.; Sargent, E. H. Efficient Ethylene Electrosynthesis through C−O Cleavage Promoted by Water Dissociation. *Nat. Synth.* **2024**, *3* (9), 1104−1112.

(12) Jiang, Z.; Ren, S.; Cao, X.; Fan, Q.; Yu, R.; Yang, J.; Mao, J. PH-Universal Electrocatalytic CO2 Reduction with Ampere-Level Current Density on Doping-Engineered Bismuth Sulfide. *Angew. Chem.* **2024**, *136* (32), No. e202408412.

(13) García de Arquer, F. P.; Dinh, C.-T.; Ozden, A.; Wicks, J.; McCallum, C.; Kirmani, A. R.; Nam, D.-H.; Gabardo, C.; Seifitokaldani, A.; Wang, X.; Li, Y. C.; Li, F.; Edwards, J.; Richter, L. J.; Thorpe, S. J.; Sinton, D.; Sargent, E. H. CO2 Electrolysis to Multicarbon Products at Activities Greater than 1 A Cm−2. *Science* **2020**, *367* (6478), 661−666.

(14) Endrődi, B.; Samu, A.; Kecsenovity, E.; Halmágyi, T.; Sebők, D.; Janáky, C. Operando Cathode Activation with Alkali Metal Cations for High Current Density Operation of Water-Fed Zero-Gap Carbon Dioxide Electrolysers. *Nat. Energy* **2021**, *6* (4), 439−448.

(15) Disch, J.; Bohn, L.; Metzler, L.; Vierrath, S. Strategies for the Mitigation of Salt Precipitation in Zero-Gap CO$_2$ Electrolyzers Producing CO. *J. Mater. Chem. A* **2023**, *11* (14), 7344−7357.

(16) Cofell, E. R.; Nwabara, U. O.; Bhargava, S. S.; Henckel, D. E.; Kenis, P. J. A. Investigation of Electrolyte-Dependent Carbonate Formation on Gas Diffusion Electrodes for CO2 Electrolysis. *ACS Appl. Mater. Interfaces* **2021**, *13* (13), 15132−15142.

(17) Sassenburg, M.; Kelly, M.; Subramanian, S.; Smith, W. A.; Burdyny, T. Zero-Gap Electrochemical CO$_2$ Reduction Cells: Challenges and Operational Strategies for Prevention of Salt Precipitation. *ACS Energy Lett.* **2023**, *8* (1), 321−331.

(18) Leonard, M. E.; Clarke, L. E.; Forner-Cuenca, A.; Brown, S. M.; Brushett, F. R. Investigating Electrode Flooding in a Flowing Electrolyte, Gas-Fed Carbon Dioxide Electrolyzer. *ChemSusChem* **2020**, *13* (2), 400−411.

(19) Moss, A. B.; Garg, S.; Mirolo, M.; Giron Rodriguez, C. A.; Ilvonen, R.; Chorkendorff, I.; Drnec, J.; Seger, B. In Operando Investigations of Oscillatory Water and Carbonate Effects in MEA-Based CO2 Electrolysis Devices. *Joule* **2023**, *7* (2), 350−365.

(20) Garg, S.; Xu, Q.; Moss, A. B.; Mirolo, M.; Deng, W.; Chorkendorff, I.; Drnec, J.; Seger, B. How Alkali Cations Affect Salt Precipitation and CO2 Electrolysis Performance in Membrane Electrode Assembly Electrolyzers. *Energy Environ. Sci.* **2023**, *16* (4), 1631−1643.

(21) Liu, Z.; Yang, H.; Kutz, R.; Masel, R. I. CO2 Electrolysis to CO and O2 at High Selectivity, Stability and Efficiency Using Sustainion Membranes. *J. Electrochem. Soc.* **2018**, *165* (15), J3371.

(22) Giron Rodriguez, C. A.; Kani, N. C.; Moss, A. B.; Joensen, B.ør. O.; Garg, S.; Deng, W.; Wilson, T.; Varcoe, J. R.; Chorkendorff, I.; Seger, B. Insights into Zero-Gap CO2 Electrolysis at Elevated Temperatures. *EES Catal* **2024**, *2* (3), 850−861.

(23) Endrődi, B.; Kecsenovity, E.; Samu, A.; Halmágyi, T.; Rojas-Carbonell, S.; Wang, L.; Yan, Y.; Janáky, C. High Carbonate Ion Conductance of a Robust PiperION Membrane Allows Industrial Current Density and Conversion in a Zero-Gap Carbon Dioxide Electrolyzer Cell. *Energy Environ. Sci.* **2020**, *13* (11), 4098−4105.

(24) Luo, T.; Abdu, S.; Wessling, M. Selectivity of Ion Exchange Membranes: A Review. *J. Membr. Sci.* **2018**, *555*, 429−454.

(25) Takagi, R.; Vaselbehagh, M.; Matsuyama, H. Theoretical Study of the Permselectivity of an Anion Exchange Membrane in Electrodialysis. *J. Membr. Sci.* **2014**, *470*, 486−493.

(26) Rumble, J. R., Jr. *CRC Handbook of Chemistry and Physics*, 103rd ed.; CRC Press/Taylor & Francis: Boca Raton, FL, 2022.

(27) Disch, J.; Bohn, L.; Koch, S.; Schulz, M.; Han, Y.; Tengattini, A.; Helfen, L.; Breitwieser, M.; Vierrath, S. High-Resolution Neutron Imaging of Salt Precipitation and Water Transport in Zero-Gap CO2 Electrolysis. *Nat. Commun.* **2022**, *13* (1), 6099.

(28) Kong, Y.; Hu, H.; Liu, M.; Hou, Y.; Kolivoška, V.; Vesztergom, S.; Broekmann, P. Visualisation and Quantification of Flooding Phenomena in Gas Diffusion Electrodes Used for Electrochemical CO2 CO$_2$ Reduction: A Combined EDX/ICP−MS Approach. *J. Catal.* **2022**, *408*, 1−8.

(29) Kato, S.; Ito, S.; Nakahata, S.; Kurihara, R.; Harada, T.; Nakanishi, S.; Kamiya, K. Quantitative Analysis and Manipulation of Alkali Metal Cations at the Cathode Surface in Membrane Electrode Assembly Electrolyzers for CO2 Reduction Reactions. *ChemSusChem* **2024**, *17* (22), No. e202401013.

(30) Joensen, B.ør. O.; Zamora Zeledon, J. A.; Trotochaud, L.; Sartori, A.; Mirolo, M.; Moss, A. B.; Garg, S.; Chorkendorff, I.; Drnec, J.; Seger, B.; Xu, Q. Unveiling Transport Mechanisms of Cesium and Water in Operando Zero-Gap CO2 Electrolyzers. *Joule* **2024**, *8* (6), 1754−1771.

(31) Petrov, K. V.; Mao, M.; Santoso, A.; Ryzhkov, I. I.; Vermaas, D. A. Design Criteria for Selective Nanofluidic Ion-Exchange Membranes. *J. Membr. Sci.* **2023**, *688*, 122156.

(32) Monteiro, M. C. O.; Dattila, F.; Hagedoorn, B.; García-Muelas, R.; López, N.; Koper, M. T. M. Absence of CO2 Electroreduction on Copper, Gold and Silver Electrodes without Metal Cations in Solution. *Nat. Catal.* **2021**, *4* (8), 654−662.

(33) Monteiro, M. C. O.; Dattila, F.; López, N.; Koper, M. T. M. The Role of Cation Acidity on the Competition between Hydrogen Evolution and CO2 Reduction on Gold Electrodes. *J. Am. Chem. Soc.* **2022**, *144* (4), 1589−1602.

(34) McCallum, C.; Gabardo, C. M.; O'Brien, C. P.; Edwards, J. P.; Wicks, J.; Xu, Y.; Sargent, E. H.; Sinton, D. Reducing the Crossover of Carbonate and Liquid Products during Carbon Dioxide Electroreduction. *Cell Rep. Phys. Sci.* **2021**, *2* (8), 100522.

(35) Reyes, A.; Jansonius, R. P.; Mowbray, B. A. W.; Cao, Y.; Wheeler, D. G.; Chau, J.; Dvorak, D. J.; Berlinguette, C. P. Managing Hydration at the Cathode Enables Efficient CO2 Electrolysis at Commercially Relevant Current Densities. *ACS Energy Lett.* **2020**, *5* (5), 1612−1618.

(36) Espinoza, C.; Kitto, D.; Kamcev, J. Counter-Ion Conductivity and Selectivity Trade-Off for Commercial Ion-Exchange Membranes at High Salinities. *ACS Appl. Polym. Mater.* **2023**, *5* (12), 10324−10333.

(37) Zhang, B.; Gao, H.; Xiao, C.; Tong, X.; Chen, Y. The Trade-off between Membrane Permselectivity and Conductivity: A Percolation Simulation of Mass Transport. *J. Membr. Sci.* **2020**, *597*, 117751.

(38) Merck. Solubility Table of Compounds in Water at Temperature. https://www.sigmaaldrich.com/NL/en/support/calculators-and-apps/solubility-table-compounds-water-temperature (accessed August 5, 2024).